Eurographics Conference on Visualization (EuroVis) (2014)
N. Elmqvist, M. Hlawitschka, and J. Kennedy (Editors)

Characterization of Blood-Flow Patterns from Phase-Contrast MRI Velocity Fields

R. van Pelt[1], A. Fuster[1,2], G. Claassen[1] and A. Vilanova[1,3]

[1]Biomedical Engineering, Eindhoven University of Technology, The Netherlands
[2]Mathematics and Computer Science, Eindhoven University of Technology, The Netherlands
[3]Electrical Engineering, Mathematics and Computer Science, Delft University of Technology, The Netherlands

Abstract

Hemodynamic information has proven valuable for analysis of cardiovascular diseases. Aberrant blood-flow patterns, for instance, often relate to disease progression. Magnetic resonance imaging enables blood-flow measurements that provide three-dimensional velocity fields during one heartbeat. However, visual analysis of these data is challenging, because of the abundance and complexity of information. Explicit feature extraction can facilitate the pattern characterization, and hence support visualization techniques to effectively convey anomalous flow areas. In this work, we improve on existing pattern matching methods that characterize blood-flow patterns in volumetric imaging data. To this end, we propose a set of helical and vortical patterns that can be parameterized by a single variable. The characterization performance is validated on both synthetic and imaging blood-flow data. Moreover, we present a comprehensive visualization based on the pattern matching results, enabling semi-quantitative assessment of the patterns in relation to the cardiovascular anatomy.

Categories and Subject Descriptors (according to ACM CCS): F.2.2 [Nonnumerical Algorithms and Problems]: Pattern matching—vector-valued, I.3.8 [Computer Graphics]: Applications—4D PC-MRI Blood-Flow

1. Introduction

An increasing body of research demonstrates the value of blood-flow information for diagnosis and treatment assessment of cardiovascular disease (CVD) [MFK*12], which is now the leading cause of death worldwide [Wor13]. Changes in the bloodstream cause remodeling of the cardiovascular morphology, and vice versa, these morphological changes affect the blood flow. Therefore, analysis of the blood flow is essential for the assessment of the cardiovascular system.

Clinical research primarily focuses on quantitative measures derived from blood-flow data, such as flow-rate and pressure. Modern phase-contrast magnetic resonance imaging (PC-MRI) enables acquisition of quantitative volumetric velocity data, typically comprising about 150x150x50 voxels, capturing blood-flow behavior in circa 25 timesteps during a heartbeat. Visual analysis reveals the evolution of various blood-flow patterns, such as vortices and helices, often related to disease progression [BB99].

To date, qualitative assessment is not performed routinely, because visual exploration remains challenging [vPV13]. Qualitative findings are difficult to communicate and document. Attempted descriptions of the complex shape and evolution of the blood-flow patterns often remain sketchy, and hence unclear and imprecise. To facilitate the characterization of the hemodynamics, we present a pattern matching approach that identifies blood-flow patterns using a given set of template patterns. In contrast to previous work, we introduce a set of template patterns that are parameterized by a single variable. This enables a convenient description of the detected blood-flow patterns. The approach is validated using synthetic flow fields, substantiating the reliability for measured data. We employ the characterization for an integral line visualization. A tailored color coding enables semi-quantitative assessment of the blood-flow patterns.

2. Related Work

Assessment of CVD is primarily based on morphology, while blood-flow information is also evidently important [MFK*12]. Understanding of intricate hemodynamics based on 4D PC-MRI velocity data requires a characterization of the flow field. Besides quantitative measures, the spatial relations are important, which requires an unambiguous

DOI: 10.2312/eurovisshort.20141158

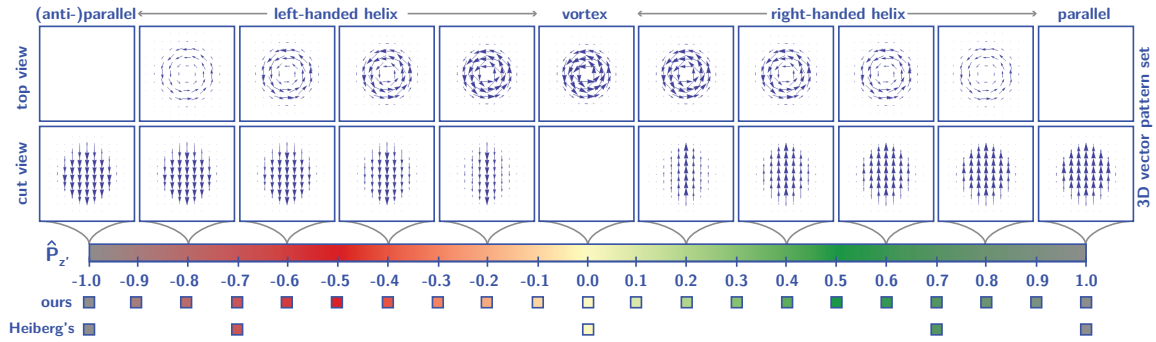

Figure 1: Our set of pattern kernels. The correspondence with the relevant patterns in Heiberg et al. [HEWK03] is shown in the axis below, in terms of the kernel component along the symmetry axis $\hat{P}_{z'}$ as described in section 3.1.

description of the blood-flow patterns. It should be noticed that blood-flow is incompressible. However, the measured 4D PC-MRI can present divergence due to limitations of the acquisition (e.g., noise).

Research aims for the flow-field topology, capturing the bare essentials using critical points [FVPF*12]. Many methods based on the velocity gradient and derived quantities have been proposed to detect vortical structures. However, all of these rely on local derivatives and are sensitive to noise in the measured data [HEWK03, ELWG14]. Moreover, topology of time-varying data remains an open challenge [PPFS10]. Instead, we search for pre-defined blood-flow patterns using a noise-robust pattern matching approach, by extending the method in [HEWK03] to locate and identify oriented flow patterns. Alternatively, Ebling et al. estimate the patterns' orientation using a Clifford convolution, and allow for a generalized pattern set [ES03].

Recent blood-flow visualizations rely on filtering of integral lines, selectively showing lines based on, e.g., maximum velocity, residence time, or vorticity [BPM*12, KGP*13]. We use the pattern matching results for our pathline visualization, using a tailored color coding that enables semi-quantitative assessment of the pattern shape.

3. Pattern Matching

3.1. Vector-valued correlation and pattern kernels

Following [HEWK03], we perform pattern matching by discrete correlation of a vector field with a vector kernel representing a certain flow pattern. The result is a similarity measure $h(\mathbf{x})$:

$$h(\mathbf{x}) = \sum_{\mathbf{x}'} \vec{P}(\mathbf{x}') \cdot \hat{D}(\mathbf{x}+\mathbf{x}') \qquad (1)$$

Here $\mathbf{x}$, $\mathbf{x}'$ denote points in the vector field and kernel domain, and $\hat{D} = \vec{D}/||\vec{D}||$ is the normalized vector (data) field. We use our own parametric description of the pattern kernels, a related parameterization can be found in [RP96]:

$$\hat{P}(\mathbf{x}',\gamma) = \frac{1}{\sqrt{(x')^2+(y')^2+\gamma^2}}(-y',x',\gamma) \qquad (2)$$

The parameter γ defines the flow pattern as a vortex ($\gamma = 0$), a right-handed helix ($\gamma = 5$) or a left-handed helix ($\gamma = -5$). Parallel flow is obtained in the limit $|\gamma| >> x', y'$. We normalize kernels such that an exact data match gives $h(\mathbf{x}) = 1$. The kernel domain/pattern size is controlled by modulating Eq. (2) by a function $f(\mathbf{x}') = \exp\{-(||\mathbf{x}'|| + R_s)/\sigma^2\}$, with σ the modulating parameter, and beyond a suppression radius R_s. We choose values $\sigma = 0.5$, $R_s = 8$ mm related to the aortic radius, which we estimated at 10 mm. Furthermore, we restrict kernel size by discarding the points with $f(\mathbf{x}'_c) < 0.01$.

We characterize patterns by the vector field component along the symmetry axis, $\hat{P}_{z'}$, evaluated at a certain reference point. This is invariant under the introduced kernel-wise normalization and modulation. We primarily aim to find patterns in the thoracic arteries, and choose the reference point $\mathbf{x}'_{\text{ref}} = (5,0,0)$, at a distance to the symmetry axis of about half the aortic radius. For example, a right-handed helix is characterized by $1/\sqrt{2}$, the z'-component of $\hat{P}(\mathbf{x}'_{\text{ref}},5) = (0,1/\sqrt{2},1/\sqrt{2})$. Similarly, $\hat{P}_{z'}(\mathbf{x}'_{\text{ref}},\gamma) = 1,1/\sqrt{2},0,-1/\sqrt{2},-1$ characterize parallel flow, a right-handed helix, a vortex, a left-handed helix and anti-parallel flow, respectively. We can now easily extend this set of patterns, by considering intermediate values of $\hat{P}_{z'}$. In this way our method, unlike Heiberg's, is sensitive to patterns with small helicity differences (see Figure 1).

3.2. Orientation estimation

For pattern matching, the kernel orientation relative to that of the data pattern should be accounted for. We compute for each kernel the similarity responses h_k in six orientations $\hat{n}_k$ pointing to vertices of a hemi-icosahedron [GK95]. A second-order orientation tensor T is then constructed as

$$T(\mathbf{x}) = \sum_{k=1}^{6} h_k^2(\mathbf{x}) \left(\frac{5}{4} \hat{n}_k^T \hat{n}_k - \frac{1}{4} I_3 \right) \qquad (3)$$

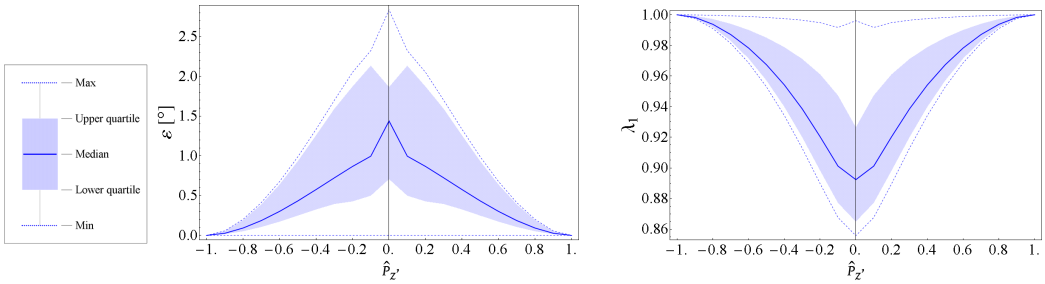

(a) (b) (c)

Figure 2: (a) Legend 'Box-whisker' graph (b) the error angle ε distribution of the orientation estimation. (c) the similarity estimation λ_1 distribution.

where I_3 is the unit matrix in 3D. The principal eigenvalue of T, λ_1, provides an estimated similarity measure, and $\lambda_1 = 1$ represents a perfect match. The corresponding eigenvector, $\hat{e}_1$, approximates the symmetry axis of the data pattern.

3.3. Voxel characterization and labeling

Each voxel is characterized by the pattern with the highest similarity measure λ_1, where we require $\lambda_1 \geq 0.8$. We group 6-connected voxels if component $\hat{P}_{z'}$ differs maximally 0.1. We then label each voxel cluster by the highest λ_1 found, and the cluster is characterized by the corresponding pattern. In the MRI data, most voxels are characterized as (anti-)parallel patterns, as expected. We regard these voxels as background, as these regions are clinically less relevant [KGP*13].

4. Validation

In this section, we validate two apects of the presented pattern matching method: the sensitivity of λ_1 to orientation changes, and its noise robustness.

4.1. Parametric vector field

We examine the relation between pattern orientation and similarity estimation, λ_1. The kernel patterns are used as synthetic data for these experiments. The data is identical to the kernels used for the pattern matching process, therefore, the result of an optimal estimation should provide $\lambda_1 = 1$. The data patterns are oriented in a total amount of 762 orientations, $\hat{s}$, distributed over the unit sphere. ε is the angle between the estimated orientation $\hat{e}_1$ and the actual data pattern orientation $\hat{s}$. $\varepsilon = 0$ indicates when $\hat{e}_1$ and $\hat{s}$ coincide.

The results of these experiments can be seen in Figure 2b and 2c. In the horizontal axes there are the different patterns presented in this paper (see Figure 1). The box-whisker chart illustrated in Figure 2a is used to present the results. The figures indicate that the orientation estimation is less accurate for patterns close to the vortex pattern, $\hat{P}_{z'} = 0$. λ_1 is also less reliable for these patterns. However, the orientation estimation accuracy increases rapidly moving towards the parallel flow, $\hat{P}_{z'} = -1$ or $\hat{P}_{z'} = 1$.

4.2. Noise robustness

In this section, we investigate if the voxels are correctly characterized under different signal to noise ratios (SNR). Given our voxel characterization method, it is important that under noisy conditions the λ_1 obtained by matching the correct pattern remains higher compared to the λ_1 obtained by non-corresponding patterns. We can also examine the validity of the threshold set at 0.8. The synthetic data used for this experiment are kernel patterns where we add Normal (Gaussian) distributed noise to the separate velocity components.

Figure 3 shows the results for having a left-handed helical pattern ($\hat{P}_{z'}$ = -0.7), and for different SNR. The measured data typically yield an SNR of about 30 [BFS*10]. The λ_1 value corresponds with a left-handed helical pattern remains the highest for all SNR levels. This trend continues in the results for all other patterns. These results provide confidence in the chosen approach regarding voxel characterization.

5. Results and Visualization

We apply our approach to 4D PC-MRI data, and account for the customary voxel size anisotropy, e.g., $2.0 \times 2.0 \times 2.5$ mm, by adopting the measured data grid as our kernel grid. We also apply a binary voxel mask, obtained by threshold-

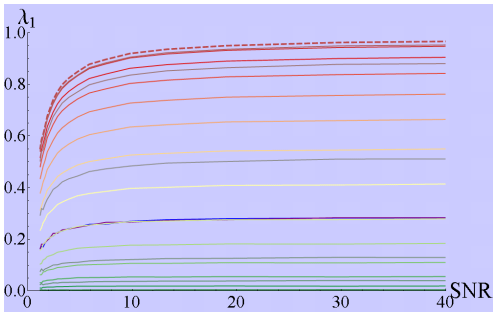

Figure 3: Similarity estimation λ_1 for the pattern $\hat{P}_{z'} = -0.7$ with different SNR. Each line represents the matching kernel, see color coding in Figure 1. The dashed line is λ_1 for the matching kernel $\hat{P}_{z'} = -0.7$.

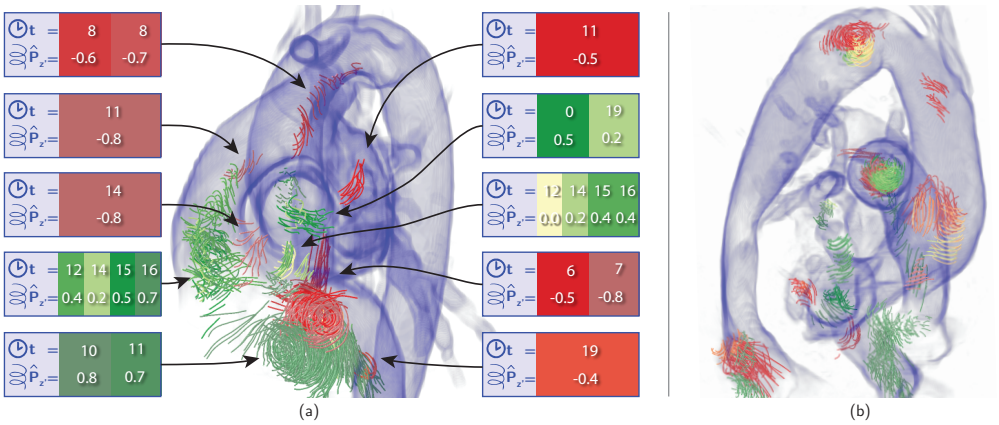

Figure 4: Pathline visualizations based on blood-flow pattern clusters in the complete cardiac cycle. (a) Volunteer data: clusters with an estimated similarity measure $\lambda_1 \leq 0.8$ and $|\hat{P}_{z'}| \leq 0.8$ (b) Dissection patient data: clusters with an estimated similarity measure $\lambda_1 \leq 0.8$ and $|\hat{P}_{z'}| \leq 0.8$ in a right-posterior view.

ing a temporal maximum intensity projection (tMIP) of the blood-flow speed over the cardiac cycle.

Based on the voxel-wise blood-flow pattern characterization, we introduce an integral-line visualization that conveys the patterns' shape and evolution. Seed points are placed in regions of the characterized patterns, and pathlines are generated forward and backward in time for a fixed duration, e.g., two timesteps. Each pathline is rendered as an imposter tuboid. A tailored color scheme enables fast interpretation of the patterns. Figure 1 shows the diverging color map. Towards vortical flow, the intensity increases to a bright yellow for a pure vortex. Towards parallel flow, the saturation decreases towards gray. Strong patterns, such as a helix or a vortex, are therefore easily identified by saturated colors.

Given the primary clinical interest in anomalous blood-flow behavior, parallel flow patterns are eliminated from the visualization. All other detected patterns throughout the heartbeat can be presented in a static representation, shown in Fig. 4. The patterns can also be depicted per time step. As a result, the visualization is an effective overview of the patterns' characteristic and shape, and enables a stability judgment of the patterns over time, as explained in Fig. 4a.

Our approach was implemented as a proof of concept with *Mathematica*. On a modern quad core system with 6GB of memory, a 4D blood-flow dataset is processed in about three hours and thirthy minutes. The interactive visualization was implemented in C++ using the OpenGL library.

6. Conclusions and Future Work

The presented pattern matching approach enables characterization of blood-flow patterns in 4D PC-MRI data. The method relies on velocity vector normalization, and is invariant to blood-flow speed. This enables detection of patterns with speed variations, e.g., during systole and diastole. In the visualization, the pathlines' length provides a visual indicator of the blood-flow speed within each pattern.

The introduced pattern set enables reliable detection of helical and vortical patterns in measured data. However, the set is not all-embracing. Constraints for orientation estimation, e.g., axis symmetry, limits the number of patterns. Diverging and converging patterns cannot be detected reliably. However, the presented set comprises the main patterns addressed in CVD clinical research, and is described by a simple parameter. $\hat{P}_{z'}$ provides an intuitive and rather accurate description of blood-flow patterns.

We have proposed a localization and characterization of blood-flow patterns, facilitating visual analysis and documentation of 4D MRI blood-flow data. A pattern set (Fig. 1), provides a set of helical and vortical patterns. The patterns are conveniently described by a single parameter, facilitating communication and documentation. Orientation of the flow pattern is computed, and although not exploided in this paper, it is potentially useful for clinical research.

The accuracy of our matching approach was assessed using parametric flow fields. The validation showed that our method is reliable under typical PC-MRI noise. Another advantage is the intuitive correspondance between our single-parameter description of patterns and their visualization. In future work it would definitely be interesting to compare both approaches, and analyse the robustness of the results to parameter settings.

A custom integral-line visualization conveys the resulting characterization using a tailored color coding of the pathlines. Visual clutter is reduced by eliminating parallel flow and, therefore, patterns of interest throughout the heartbeat can be conveyed in a static representation (Fig. 4). In the future, computation time can be improved by a optimized and parallel implementation. Also, it is worthwhile investigating a spatiotemporal pattern matching approach, capturing the inherent unsteady nature of blood-flow dynamics.

References

[BB99] BOGREN H. G., BUONOCORE M. H.: Complex flow patterns in the great vessels: a review. *Journal of Cardiac Imaging 15*, 2 (1999), 105–113. 1

[BFS*10] BOCK J., FRYDRYCHOWICZ A., STALDER A. F., BLEY T. A., BURKHARDT H., HENNIG J., MARKL M.: 4d phase contrast mri at 3 t: Effect of standard and blood-pool contrast agents on snr, pc-mra, and blood flow visualization. *Magnetic Resonance in Medicine 63*, 2 (2010), 330–338. 3

[BPM*12] BORN S., PFEIFLE M., MARKL M., GUTBERLET M., SCHEUERMANN G.: Visual Analysis of Cardiac 4D MRI Blood Flow Using Line Predicates. *IEEE Transactions on Visualization and Computer Graphics* (2012), 1–14. 2

[ELWG14] ELBAZ M., LELIEVELDT B., WESTENBERG J., GEEST R.: Automatic extraction of the 3D left ventricular diastolic transmitral vortex ring from 3D whole-heart phase contrast MRI using Laplace-Beltrami signatures. In *Statistical Atlases and Computational Models of the Heart. Imaging and Modelling Challenges*, Camara O., Mansi T., Pop M., Rhode K., Sermesant M., Young A., (Eds.), vol. 8330 of *Lecture Notes in Computer Science*. Springer Berlin Heidelberg, 2014, pp. 204–211. 2

[ES03] EBLING J., SCHEUERMANN G.: Clifford convolution and pattern matching on vector fields. In *IEEE Visualization* (2003), pp. 193–200. 2

[FVPF*12] FUSTER A., VAN PELT R., FICK R., CLAASSEN G., TER HAAR ROMENY B., VAN ASSEN H., FLORACK L.: 3D saddle point detection and applications in cardiac imaging. In *Biomedical Imaging (ISBI)* (2012), pp. 808–811. 2

[GK95] GRANLUND G. H., KNUTSSON H.: *Signal Processing for Computer Vision*. Kluwer Academic Publishers, 1995. ISBN 0-7923-9530-1. 2

[HEWK03] HEIBERG E., EBBERS T., WIGSTROM L., KARLSSON M.: Three-dimensional flow characterization using vector pattern matching. *IEEE Transactions on Visualization and Computer Graphics 9*, 3 (2003), 313–319. 2

[KGP*13] KÖHLER B., GASTEIGER R., PREIM U., THEISEL H., GUTBERLET M., PREIM B.: Semi-Automatic Vortex Extraction in 4D PC-MRI Cardiac Blood Flow Data using Line Predicates. *IEEE Transactions on Visualization and Computer Graphics 19*, 12 (2013), 2773–2782. 2, 3

[MFK*12] MARKL M., FRYDRYCHOWICZ A., KOZERKE S., HOPE M., WIEBEN O.: 4D flow MRI. *Journal of Magnetic Resonance Imaging 36*, 5 (2012), 1015–1036. 1

[PPFS10] POBITZER A., PEIKERT R., FUCHS R., SCHINDLER B.: On the way towards topology-based visualization of unsteady flow - the state of the art. In *Eurographics STARs* (2010), pp. 137–154. 2

[RP96] ROTH M., PEIKERT R.: Flow Visualization for Turbomachinery Design. In *Proceedings IEEE Visualization 1996* (Los Alamitos, CA, USA, 1996), IEEE Computer Society Press, pp. 381–384. 2

[vPV13] VAN PELT R., VILANOVA A.: Understanding Blood-Flow Dynamics: Challenges in Visualization. *IEEE Computer 46*, 12 (2013), 60–67. 1

[Wor13] WORLD HEART ORGANIZATION: Fact sheet CVD. http://www.who.int/mediacentre/factsheets/fs317/ (last visited 11/12/2013), 2013. 1